28

Pioneering Applications of Two-Photon Microscopy to Mammalian Neurophysiology

Seven Case Studies

Q.-T. Nguyen, G. O. Clay, N. Nishimura, C. B. Schaffer, L. F. Schroeder, P. S. Tsai, and D. Kleinfeld

It is commonly assumed, although insufficiently acknowledged, that major advances in neuroscience are spurred by methodological innovations. Novel techniques may appear quite daunting at first, but their successful application not only places them among mainstream methods, but also stimulates further developments in new directions. Such is the case for two-photon laser scanning microscopy (TPLSM) (Denk et al., 1990), which was introduced in neuroscience in the early 1990s (Denk et al., 1994). Since that time, the impact of TPLSM in neurobiology has been nothing short of remarkable. Several excellent reviews on TPLSM have already covered the general aspects of this technique (Denk et al., 1995; Denk & Svoboda, 1997; Stutzmann and Parker, 2005; Zipfel et al., 2003), details of the instrumentation (Tsai et al., 2002), and recent advances (Brecht et al., 2004). The object of this chapter is to showcase seminal applications of TPLSM in neuroscience, with a particular emphasis on mammalian neurobiology. The seven case studies presented here not only expound the broad range of applications of TPLSM but also show that TPLSM has been used to resolve significant issues in mammalian neurobiology that were previously unanswered due to lack of an appropriate technique.

28.1 QUALITATIVE BACKGROUND

The inherent qualities of TPLSM that have allowed groundbreaking advances in neuroscience derive entirely from using a high-repetition-rate mode-locked laser, typically a femtosecond pulsed Ti:Sapphire oscillator. This device generates trains of intense short light pulses ($\leq$100 fs) at rates ranging from a few kilohertz to one gigahertz. Although the average power of a femtosecond laser in a TPLSM is in the order of a few hundred milliwatts or less, the density of incident photons during each pulse is such that fluorophores that are normally excited by photons with wavelength λ (energy hc/λ, where h is Planck's constant and c is the speed of light) can be excited by the near-simultaneous

HBNOM: "CHAP28" — 2007/10/13 — 16:39 — PAGE 715 — #9

arrival of two photons with double the wavelength and half the energy. The probability that the nonlinear, two-photon absorption process occurs will increase as the square of the intensity of the incident light.

Two-photon laser scanning microscopes provide images with a resolution markedly better than that of wide-field fluorescence microscopes in scattering samples; a comparison between nonlinear and confocal imaging techniques with the same preparation is given by Kang and colleagues (Kang et al., 2005). Two-photon laser scanning microscopes take advantage of the square dependence of two-photon absorption with excitation intensity by tightly focusing the laser beam with a high numerical aperture (NA) objective. This creates a volume of less than 1 μm^3 in which two-photon excitation takes place. The resulting natural optical sectioning effect allows micrometer to submicrometer resolution in three dimensions. A volume is probed by sweeping the focal point of the beam. Within the focal plane, this is achieved by systematically varying the incident angle of the laser beam in the back-aperture of the objective with galvanometric mirrors (Tan et al., 1999), resonant fiber optics (Helmchen et al., 2001), or acousto-optical deflectors (Bullen et al., 1997; Roorda et al., 2004). Between planes, this is achieved by changing the height of the objective relative to the sample.

The confinement of excitation in TPLSM is particularly advantageous for neurobiological applications. First, the small excitation volume alleviates fluorophore bleaching or phototoxic damages outside the focal plane. This feature is critical for long-term time-lapse imaging of cellular morphology or observation of neuronal activity in subcellular compartments. Second, the small excitation volume greatly reduces out-of-focus absorption due to scattering of incident photons, which is advantageous when imaging deep inside a specimen. Incidentally, the ability to optically section solely with the incident beam simplifies the design of two-photon microscopes in comparison with conventional laser confocal scanning systems.

Of considerable importance for in vivo neurobiological imaging applications is the use of laser wavelengths that fall in the near-infrared range. Photons in these wavelengths are better able to penetrate neural tissue, which is heavily scattering, than photons with shorter wavelengths. Consequently, excitation light that is generated by common femtosecond lasers can reach several hundred of microns under the surface of the brain while still being able to excite fluorescent molecules that are normally stimulated with shorter wavelengths. This was particularly apparent in the case of astrocytes imaged in a brain slice (Kang et al., 2005), where TPLSM provided excellent resolution of cells as deep as 150 μm inside the specimen, while imaging with a laser confocal microscope was limited to the immediate surface of the neural tissue and was further hampered by phototoxicity.

28.2 IN VITRO SUBCELLULAR APPLICATIONS OF TPLSM

TPLSM was first employed to measure calcium dynamics in subcellular compartments of single neurons with unprecedented spatial resolution (Kaiser et al., 2004; Noguchi et al., 2005; Svoboda et al., 1996; Yuste & Denk, 1995). These experimental results bear on theories that associate activity-dependent, long-lasting cognitive processes such as learning and memory with possible physiological and anatomical changes in brain cells. It has been proposed that in certain categories of neurons, subcellular

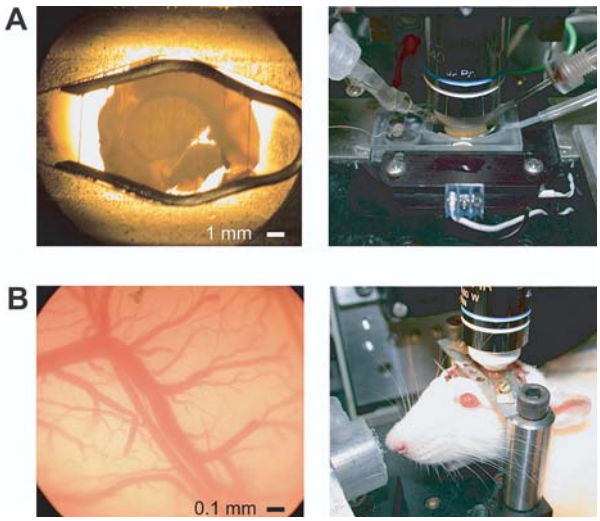

Figure 28.1. In vitro and in vivo mammalian preparations used in neurobiological experiments involving TPLSM. (A) Brain slice preparation. Left picture: 400-μm thick slice from the forebrain of an adult rat. The slice was placed in a recording chamber and held in place by an anchor with nylon threads straddling the slice. Right picture: Optical/electrophysiological recording setup with an extracellular stimulating electrode on the left and an intracellular recording electrode on the right. (B) Anesthetized rodent preparation. Left picture: Bright-field image of the vasculature at the surface of the cerebral cortex of a rat viewed through the imaging craniotomy. Bottom picture: In vivo recording setup. Notice the optical window placed above the craniotomy and under the microscope objective. The nose of the rat is facing a nozzle providing a constant flow of anesthetic.

appendages present on neuronal extensions, called dendritic spines, play a central role in the integration of input signals coming from other neurons. Further, many theories posit that dendritic spines are essential in memory formation and storage (Martin et al., 2000). The geometry and size of dendritic spines could, in principle, allow local retention of calcium, an ion known to be critical for many long-term intracellular events. However, basic physiological properties of dendritic spines could not be measured prior to the advent of TPLSM since the volume of dendritic spines is in the order of one cubic micrometer or less. Seminal experiments on dendritic spines using in vitro brain slice preparations (Fig. 28.1A) were among the first applications of TPLSM in neurobiology (Svoboda et al., 1996; Yuste & Denk, 1995). Calcium regulation in subcellular compartments is still a much-studied topic with TPLSM (Kaiser et al., 2004), sometimes in combination with two-photon activation of caged neurotransmitters (Noguchi et al., 2005).

28.3 IN VIVO CELLULAR APPLICATIONS OF TPLSM

It was quickly realized that the ability to use TPLSM to image deep inside neural tissue would allow investigators to link neuronal activity and morphology at higher levels of organization in the brain. It has long been proposed that the connectivity of neural circuits is not fixed but varies according to the pattern of its inputs. TPLSM was used

to validate this hypothesis in vitro (Engert & Bonhoeffer, 1999; Maletic-Savatic et al., 1999). Experimental evidence of activity-dependent remodeling of neuronal wiring in response to sensory manipulation was provided by TPLSM imaging in the cerebral cortex of developing rats (Grutzendler et al., 2002; Lendvai et al., 2000; Trachtenberg et al., 2002).

The ability to image deep inside the brain of live, anesthetized animals has opened the way to record the electrical activity of whole neural networks using TPLSM (see Fig. 28.1B), providing that neurons in these networks are loaded with an appropriate optical reporter. Calcium-sensitive fluorescent dyes (Grynkiewicz et al., 1985) are currently the indicators of choice because their fluorescence varies robustly with changes in the concentration of intracellular calcium that, in turn, is strongly correlated with neuronal activity. Furthermore, many calcium-sensitive fluorescent dyes exist in a cell-permeant form, which facilitates their entry into neurons. However, a recurrent problem in in vivo experiments is the ability to label potentially thousands of cells of interest with intracellular dyes in a volume that corresponds to the extent of the network of interest. A method that involves intracerebral perfusion of dyes is described by Stosiek and colleagues (Stosiek et al., 2003). Using this approach, Ohki and coworkers managed to accurately map domains of common neuronal responses involved in vision in the adult rat cerebral cortex (Ohki et al., 2005). Other labeling approaches include the use of modified, nonpathogenic viruses to deliver a genetically engineered fluorescent dye (Lendvai et al., 2000) and the development of transgenic mice that express a fluorescent protein in specific neurons (Margrie et al., 2003). In the latter case, labeled cells correspond to neurons with a unique phenotype. These cells can be unequivocally localized and targeted for intracellular microelectrode recording under visual control provided by TPLSM (Margrie et al., 2003).

28.4 TPLSM FOR HEMODYNAMIC AND NEUROPATHOLOGIC ASSESSMENTS

The coupling between blood flow and neuronal activity is, at present, only partially understood. TPLSM provides a tool to aid studies in this area. Fluorescent dye injected into the bloodstream acts as a contrast agent, allowing TPLSM to visualize the motion of red blood cells. This technique provides a straightforward means to measure cerebral blood flow in vivo (Chaigneau et al., 2003; Kleinfeld, 2002; Kleinfeld et al., 1998). A related application of TPLSM is to study neurovascular diseases in animal models. For example, TPLSM in combination with neuropathological markers has been used to monitor the progression of Alzheimer's disease in a minimally invasive fashion before and after immunological treatment (Backsai et al., 2001, 2002). The proven ability of TPLSM to monitor the effectiveness of potential cures for a major neurodegenerative disease in vivo highlights the potency and versatility of this technique.

28.4.1 Case Studies of the Application of TPLSM to Mammalian Neurophysiology

We consider seven case studies highlighting novel findings in mammalian neurophysiology that relied on TPLSM. These serve to illustrate the power of the technique, as

well as the importance of correlating TPLSM-based observations with measurements performed with other techniques such as intracellular electrophysiology. Our examples range from subcellular dynamics to population responses.

28.4.1.1 Calcium Dynamics in Dendritic Spines

Two-photon imaging is a particularly powerful tool to study neural activity at the scale of individual dendrites and dendritic spines in vitro. These experiments are performed in brain slice preparations (see Fig. 28.1A). Brain slices are obtained by cutting specific regions of isolated brains, such as the hippocampus, into sections with a thickness usually ranging from 100 to 500 μm. When brain slices are bathed in the appropriate saline, neurons remain viable and their connections can be functional for several hours. An important advantage of optical experiments done in brain slices is the absence of biological motion artifacts, such as respiration or heartbeat. The thinness of brain slices is also advantageous in many respects, while the relative transparency of slices and their flatness facilitates optical imaging. Pharmacological compounds such as ion channel blockers have better access to their target than in the whole brain. Finally, intracellular recordings in slices are much easier to perform and more stable than those in vivo.

The size of spines is on the order of what can be resolved with diffraction-limited optical imaging. Thus, dynamic studies of spine morphology and physiology require the ability to image with micrometer-scale resolution into a highly scattering sample. This requirement is met by TPLSM used in conjunction with fluorescent probes that are sensitive to the intracellular environment. Yuste and Denk (Yuste & Denk, 1995) injected single neurons in brain slices with the calcium-sensitive dye Calcium Green and monitored fluorescence changes in individual spines and the contiguous dendritic shafts in response to electrical stimulation. TPLSM enabled them to resolve individual spines and the shaft between the spines. Stimulation of the cell soma elicited calcium changes in individual spines via opening of local calcium channels (Figs. 28.2A and 28.2B), definitively establishing that the dendritic spine serves as a basic unit of computation in the mammalian nervous system. A key result of this study was that the confluence of presynaptic and postsynaptic spiking led to a nonlinear enhancement in the concentration of intracellular calcium within the postsynaptic spine.

Kaiser and colleagues (Kaiser et al., 2004) extended the approach of Yuste and Denk (1995) by injecting two connected neurons with calcium-sensitive fluorescent dyes with different emission wavelengths. They subsequently identified a synaptic connection between the axon of one neuron and one dendrite on the other neuron based on cellular morphology. Since the calcium dyes labeling either side of the synapse were spectrally distinct, the authors were able to independently identify the calcium dynamics on the presynaptic and postsynaptic side of the neural connection (see Figs. 28.2C to 28.2E).

28.4.1.2 Structure–Function Relationship of Dendritic Spines

Fundamental characterization of dendritic spine properties can be carried further by combining imaging with other optical processes that utilize the spatial confinement

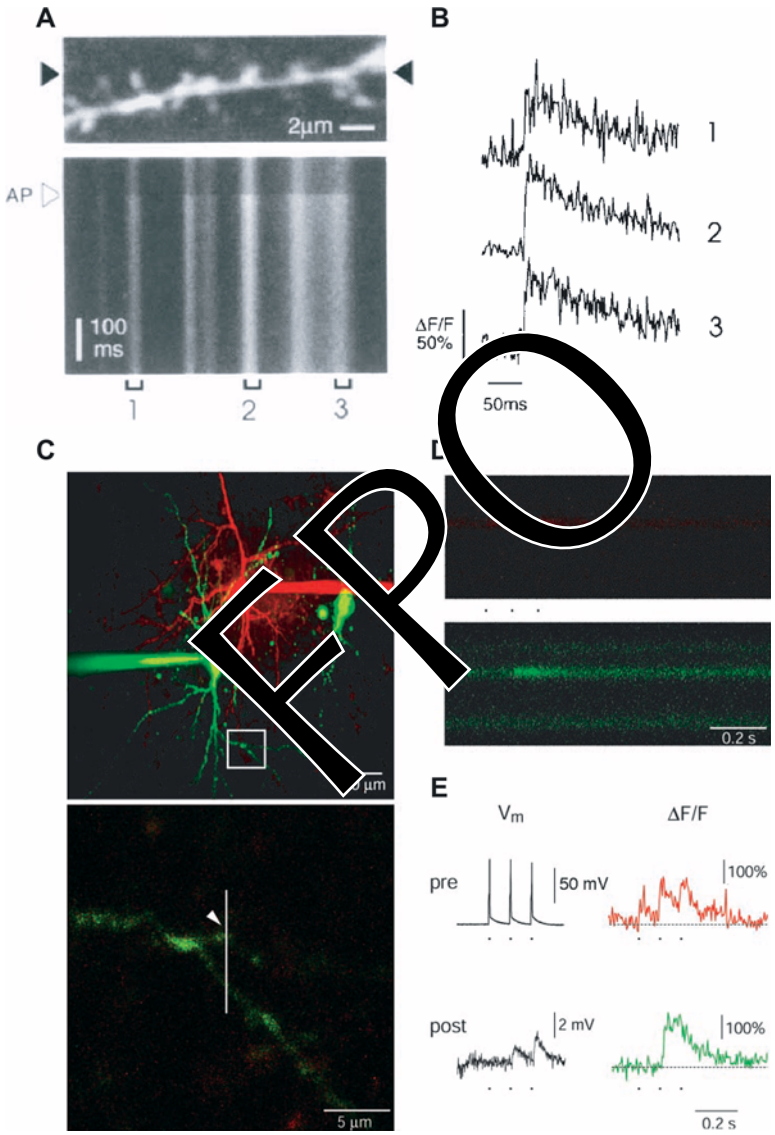

Figure 28.2. Subcellular calcium dynamics in neurons imaged by TPLSM. (A) Image of dendritic segment of a neuron labeled with the calcium-sensitive fluorescent dye Calcium Green (top) and repetitive line-scans between black arrows (bottom) during an action potential elicited by a 3-ms, 50-mV pulse applied to the soma (white arrow in line-scan data). Increases in fluorescence, associated with increases in calcium ion concentration, were observed in all dendrites. (B) Fluorescence changes in three dendritic spines as a function of time. In contrast to these data, the calcium ion transients induced by stimulation that was not sufficient to generate an action potential resulted in measurable calcium ion concentrations only in a subset of dendritic spines. (C) Two-photon fluorescence image (top) of a pyramidal neuron (red, labeled with Rhodamine-2) and a bitufted interneuron (green, labeled with Oregon Green Bapta-1). For both dyes, the fluorescence increased with increases in calcium ion concentration. Image of a synapse (bottom) between the pyramidal cell and the interneuron, from the region in panel A, indicated with a white box. The arrowhead indicates the location of the synapse, and the white line indicates the region where the line-scan data shown in panel D were taken.

of two-photon interactions. Photobleaching and photoactivation processes that result from two-photon absorption can be used to induce and observe dynamics with a spatial resolution sufficient to study subcellular structures. In work by Svoboda and associates (Svoboda et al., 1996), dendrites of neurons in rat hippocampal slices were loaded with fluorescein-dextran via an intracellular micropipette. TPLSM enabled visualization of individual spines in neurons inside the optically scattering brain slice (see Fig. 28.1A). The authors achieved the necessary time resolution to image diffusion through the use of a line-scan pattern, in which the focus of the femtosecond laser beam was repeatedly scanned along a single line through the spine or dendrite of interest (Figs. 28.3A to 28.3C). The time resolution was determined by the speed of the scanning mirrors, which was $\sim$2 ms/line in these experiments. During line-scan imaging, fluorescein in either the dendrite or synapse was photobleached or photoreleased by a high laser power during a single line scan. The subsequent recovery of fluorescence or decrease of fluorescence was used as a measure of the diffusion between the unbleached and bleached areas. The use of different combinations of photobleaching and imaging in the spine and its dendritic shaft enabled the authors to demonstrate that chemical compartmentalization takes place in spines, and to estimate the electrical resistance of the spine neck.

The role of specific components involved in synaptic signaling, such as NMDA (N-methyl-d-aspartate) receptors, can also be investigated using TPLSM. Presynaptic neurons transform their electrical activity into the release of packets of neurotransmitter molecules, which will target cells across the synapse. NMDA receptors are protein complexes located on the postsynaptic side of a synapse that transduce pulses of the neurotransmitter glutamate into excitatory electrical potentials in the postsynaptic cell. NMDA receptors are thought to be critical for neuronal plasticity because of their additional dependence of the postsynaptic voltage and their large permeability to calcium, which leads to an increase in intracellular calcium in the postsynaptic cell when NMDA receptors are activated. Localized glutamate release can be mimicked in vitro by using caged glutamate, an inert derivative of glutamate that can release ("uncage") glutamate when it is optically activated by absorption of a UV photon or, equivalently, by two photons in the visible range.

Noguchi and colleagues (Noguchi et al., 2005) combined two-photon fluorescence imaging of a calcium indicator with two-photon photon-uncaging of glutamate to understand the role of calcium signaling during NMDA receptor activation in hippocampal

---

Figure 28.2 (*Continued*). (D) Line-scans taken during the stimulation of three action potentials in the presynaptic, pyramidal neuron (top) and the postsynaptic interneuron (bottom). Three action potentials were evoked in the pyramidal cell, giving rise to a calcium ion increase in the presynaptic cell (top image). (E) Electrical recordings of action potentials in the cell soma (left) and changes in fluorescence measured in a single synapse induced by calcium dynamics (right) in the presynaptic (top) and postsynaptic (bottom) cell. Three action potentials were induced in the presynaptic cell, giving rise to three transient increases in calcium ion concentration. In the postsynaptic cell, two excitatory postsynaptic potentials were measured, but only one led to a measured increase in calcium ion concentration (perhaps indicating the presence another synaptic contact between these two cells). (A and B adapted from Yuste & Denk, 1995; C-E adapted from Kaiser et al., 2004)

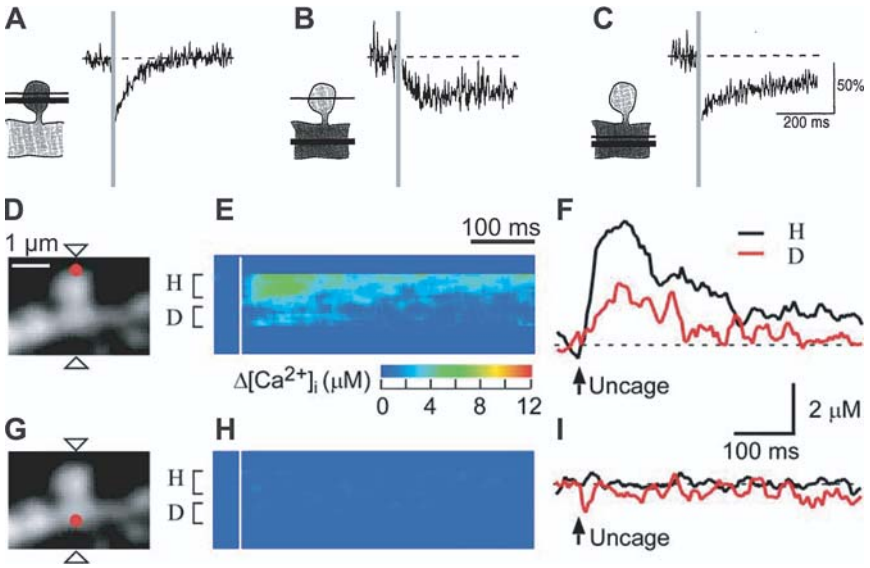

Figure 28.3. Two-photon imaging of diffusion dynamics in dendritic spines. (A–C) Photobleaching and diffusional recovery of fluorescence. Schematics indicate the position of fluorescence measurement (thin line) and photobleaching (thick lines) through spines and associate dendritic shafts. Graphs show the time course of fluorescence before and after photobleaching, indicated by gray bar. (D–I) Measurement of calcium concentration in response to stimulation by photo-uncaging glutamate. Red dots indicate position of uncaging of glutamate and arrowheads indicate position of line-scan for fluorescence signal on stacked images of spines filled with Alexa Fluor 594 (D, G). (E–H) Changes in calcium concentration derived from line-scan images of fluorescence of calcium-sensitive Oregon Green-BAPTA-5N, with bar indicating time of glutamate uncaging. H and D show regions average for F and I. (A–C adapted from Svoboda et al., 1996, D–H from Noguchi et al., 2005)

slices. Two-photon uncaging of glutamate allowed the precise excitation of NMDA receptors on a single spine head, unlike previous attempts that used electrical stimulation and failed to confine electrical excitation to individual synapses. The combination of optical activation of single synapses with an optical measurement of intracellular calcium enabled them to measure calcium changes that were induced by photochemical stimulation of a single synapse and the attached dendritic shaft. Calcium concentration was estimated with the calcium-sensitive fluorescent dye Oregon Green, and individual neurons were filled with a mixture of both calcium-sensitive and calcium-insensitive fluorescent dye. Both probes were excited with 830-nm femtosecond laser light, but their emission spectra were far enough apart to determine changes in calcium concentration via the ratio of emitted light. A second femtosecond laser at 720-nm wavelength was used to photo-uncage glutamate. Electrical current generated by the influx of ion inside the cell was also measured by conventional microelectrode intracellular recording (see Figs. 28.3D to 28.3I). Combined with pharmacological blockage of various NMDA receptors, these experiments determined that excitation of a single synapse does lead to calcium increases in the dendritic shaft, and suggested that the extent of the calcium movement between synapse and dendrite depended on the shape of the spine head and neck (see Figs. 28.3E to 28.3H).

28.4.1.3 Activity-Dependent Plasticity of the Neuronal Architectonics

Persistent changes in neuronal circuitry in response to varying inputs may occur by at least three different mechanisms: dendritic and axonal extension and pruning (Martin et al., 2000), synapse formation and elimination (Ramón y Cajal, 1893), and potentiation or depression of existing synapses (Ziv & Smith, 1996). Testing these hypotheses ideally requires that one observe a single neuron over periods of time that range from seconds to months. Early attempts to image morphological changes in peripheral neurons used wide-field microscopy (Purves & Hadley, 1985). These efforts were hampered by the poor z-axis spatial resolution inherent to conventional fluorescence imaging. In contrast, TPLSM offers the ability to image individual neurons over several months, with sufficient resolution to track changes in neuronal morphology as small as dendritic spines.

The cerebral cortex of mice includes a region called the vibrissa (whisker) somatosensory cortex, where sensory neurons are organized into functional maps that correspond to the grid-like organization of the large vibrissae on the face of the animal (Woolsey & van der Loos, 1970). Trachtenberg and coworkers (Trachtenberg et al., 2002) were able to image individual green fluorescent protein (GFP)-expressing neurons in this region over many days. They found that axons and dendrites were remarkably stable over several months. However, the morphological changes in spines varied according to three time scales: transient ($<$1 day), semi-stable (2 to 7 days), and stable ($>$8 days) (Figs. 28.4A to 28.4E). Interestingly, the evolution of spine morphology is not the same in all regions of cerebral cortex. Grutzendler and colleagues (Grutzendler et al., 2002) performed a similar study in the visual cortex of adult mouse on the same layer 2/3 dendritic arbors using TPLSM and found that 98% of the spines were stable over days and 82% were stable over months (see Fig. 28.4F).

Trachenberg and coworkers (Trachenberg et al., 2002) further assessed spine turnover in response to sensory stimulation of the vibrissae. The investigators trimmed every other vibrissa from the mystacial pad of the mouse, such that each trimmed vibrissa was surrounded by untrimmed vibrissae. This chessboard deprivation is known to produce a robust rearrangement of the cortical neuronal map of the sensory responses to individual vibrissae. The results from this study showed an increase in the turnover of spines a few days after trimming, suggesting a role for spine formation/elimination in rewiring cortical circuits (see Fig. 28.4G).

28.4.1.4 Calcium Imaging of Populations of Single Cells

While calcium imaging of individually loaded cells has yielded important insights into the calcium dynamics and neural activity in single cells, the bulk loading of cell populations with calcium indicator dyes has been, until recently, problematic for in vivo studies. The ability to load tens to hundreds of cells in a local population in vivo was demonstrated by Stosiek and associates (Stosiek et al., 2003) using a pressure-ejection method they called multicell bolus loading. In brief, a micropipette filled with dye-containing solution was placed deep in rodent cortex and was used to pressure-eject $\sim$400 fl of dye into the extracellular space (Fig. 28.5A). This resulted in a $\sim$300-μm-diameter spherical region of stained cells (see Fig. 28.5B). Using this

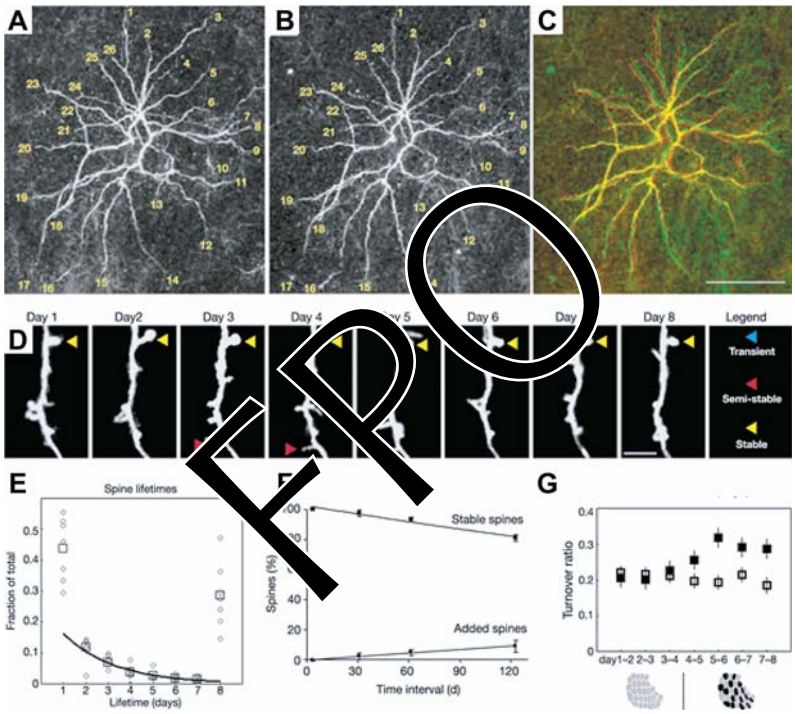

Figure 28.4. Long-term in vivo imaging of neuronal structure. (A–C) Adult mouse dendritic branches were stable over weeks. (A) Dorsal view of an apical tuft at imaging day 16; 26 branch tips are labeled for reference. (B) Imaging day 32. (C) Overlay (day 16, red; day 32, green). Scale bar, 100 μm. (D) Images of a dendritic segment acquired over eight sequential days. Spines appeared and disappeared with broadly distributed lifetimes. Examples of transient, semi-stable, and stable spines (with lifetimes of 1 day, 2 to 7 days, and 8 days, respectively) are indicated with blue, red, and yellow arrowheads, respectively. Scale bar, 5μm. (E) Spine lifetimes in adult mouse barrel cortex. Lifetimes are defined as the number of sequential days (from a total of eight) over which a spine existed. Individual neurons (gray diamonds) and the average (black squares) are shown. The fraction of spines with lifetimes of 2 to 7 days was fitted with a single time constant (thick black line). The fractions of spines with lifetimes of less than 1 day (transient spines) and greater than 8 days (stable spines) were significantly greater than predicted from the exponential fit, and therefore constitute distinct kinetic populations. (F) Spine lifetimes in adult mouse visual cortex. Percentage of spines that remained stable or were added as a function of imaging interval. Data are presented as mean ±SD. Scale bars, 1 mm. (G) Sensory experience modulated spine turnover ratio (the fraction of spines that turn over between successive imaging sessions). Chessboard deprivation of whiskers occurred immediately after imaging day 4. Turnover ratio increased after deprivation within (solid squares) but not outside (open squares) the barrel cortex. Error bars show SEM. (A–E and G adapted from Trachtenberg et al., 2002, F from Grutzendler et al., 2002)

method, cells could be loaded with a variety of membrane-permeant calcium indicators, although at lower indicator concentrations compared to cells individually loaded by intracellular injections (i.e., <100 μM compared to a few millimolar, respectively). Nonetheless, spontaneous calcium transients could be recorded optically with TPLSM from a population of cells (see Fig. 28.5C).

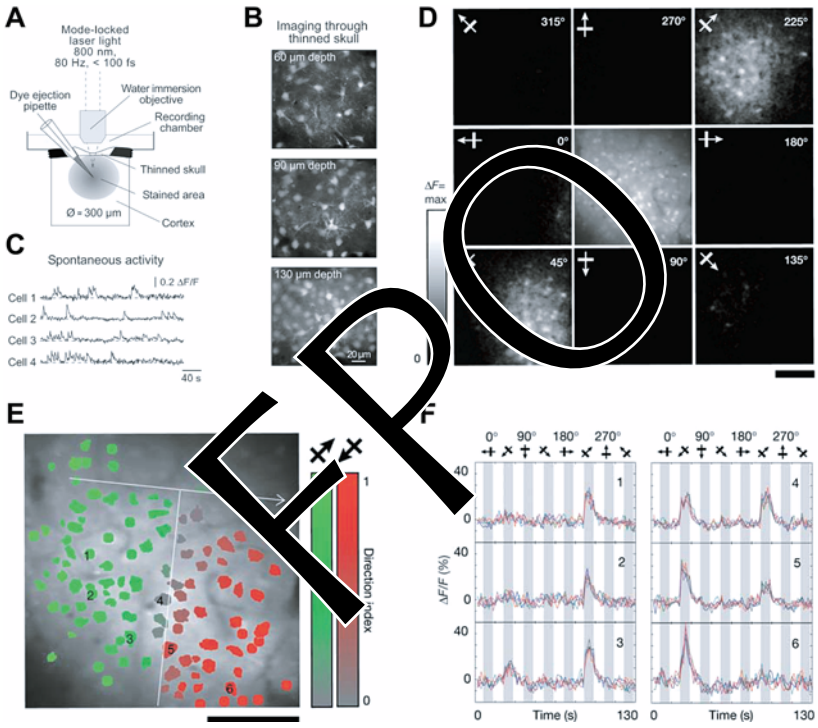

Figure 28.5. Neuronal network activity imaged by TPLSM. (A) Experimental arrangement for pressure-ejection loading of a neuronal population with a calcium indicator in vivo. (B) Images taken through a thinned skull of a P13 mouse at increasing depth after pressure-ejection loading with calcium indicator Fura-PE3 AM. (C) Spontaneous Ca^{2+} transients recorded in a different experiment through a thinned skull in individual neurons (P5 mouse) located 70 m below the cortical surface, after loading with calcium indicator Calcium Green-1 AM. Scale bar = 20 μm. (D) Direction discontinuity in cat visual cortex visualized by population loading of cells with calcium indicator in vivo, and visual stimulation with drifting square wave gratings at different orientations. Single-condition maps (ΔF) imaged 180 μm below the pia mater layer are shown in the outer panels. The central panel shows an anatomical image reconstructed by averaging over all frames during the visual stimulation protocol. Cells were activated almost exclusively by stimuli of one orientation moving in either direction (45 degrees and 225 degrees). To the non-preferred stimuli, such as 90 degrees, the calcium responses were so small and the noise was so low that the single-condition maps are almost indistinguishable from zero. Scale bar = 100 μm. (E) Cell-based direction map; 100% of cells had significant responses. Color specifies preferred direction (green, 225 degrees; red, 45 degrees). The cells responding to both 45 degrees and 225 degrees are displayed as gray, according to their direction index (see color scale on right). The vertical white line below the arrow indicates approximate position of the direction discontinuity. Scale bar = 100 μm. (F) Single-trial time courses of six cells, numbered 1 to 6 as in part E. Five trials (out of ten) are superimposed. (A–C adapted from Stosiek et al., 2003, D–F adapted from Ohki et al., 2005)

The ability to quickly and simultaneously load an entire population of cells with a functional fluorescent indicator opens the door to optical evaluation of network dynamics and functional architecture. Previously, such studies were largely limited to the use of multisite electrodes, voltage-sensitive dyes, or intrinsic optical imaging of the hemodynamic response to neuronal activity. In the case of multisite electrode recordings, the recording sites are tens to hundreds of microns apart, and hence provide only sparse sampling of a cell population. Conversely, voltage-sensitive dyes and intrinsic optical imagining have insufficient spatial resolution to distinguish the activation of individual cells in vivo.

The use of calcium indicator imaging to elucidate functional architecture was demonstrated by Ohki and associates (Ohki et al., 2005) in cat visual cortex. A population of cells was loaded with the AM form of a calcium indicator using multicell bolus loading (see Fig. 28.5D). The AM form is permeant through the cell membrane and then is trapped inside the cell (Grynkiewicz et al., 1985). The response of individual cells to visual stimuli at different orientations was characterized. It was found that sharp boundaries existed between cell populations with different tunings to oriented bars in the visual field (see Fig. 28.5E). Importantly, single-cell resolution of neuronal activity over a population of cells in vivo, as demonstrated by the response curves in Figure 28.5F, enabled investigations of the local heterogeneity in cell populations and the precision and sharpness of cortical maps.

28.4.1.5 Targeted Intracellular Recording In Vivo

The state of a neuron is represented by many dynamic variables, including intracellular calcium (see above) and other chemical species. However, the state variable closely tied to neuronal input/output relations is the transmembrane voltage. The current lack of suitable optical indicators of membrane voltage with rapid kinetics and sufficient signal-to-noise ratio precludes the use of TPLSM to replace conventional, direct measurement of membrane potential using intracellular microelectrodes. However, TPLSM is particularly useful as a tool to target specific neurons for intracellular recording in the brain of mammals in vivo, a technique that was not possible until recently.

Traditionally, a microelectrode is inserted in the brain, literately "blindly," until it contacts and then penetrates a cell. During the recording session, the neuron is filled with a dye through the micropipette. Classification of the cell phenotype is done postmortem using the position and morphology of the cell, which are determined using standard, albeit laborious, histological techniques. As demonstrated by Margrie and coworkers (Margrie et al., 2003), in vivo intracellular recordings could be drastically improved by combining transgenic mice that expressed an intrinsic fluorescent indicator in a specific population of neurons and TPLSM, which allowed precise visualization of these cells in the z-plane.

Margrie and coworkers (Margrie et al., 2003) specifically targeted cortical inhibitory interneurons. These are small cells that do not have a stereotypical pattern of electrical activity that would make them identifiable using "blind" intracellular or extracellular recording techniques. The animals belonged to a strain of mice that was genetically altered so that their cortical inhibitory interneurons selectively expressed GFP, an exogenous protein. Mice were prepared with a cranial window covered with a recording

chamber filled with agarose to dampen cardiovascular pulsations of the cortex. The chamber had an edge open on one side to allow insertion of an electrode at an oblique angle. TPLSM was used to visualize a targeted interneuron and to guide the intracellular recording microelectrode. To facilitate its localization, the electrode was filled with a fluorescent dye that was also excited by the laser but emitted in a different color than that of the labeled cells (Fig. 28.6A). Proof that the electrode had penetrated and thus

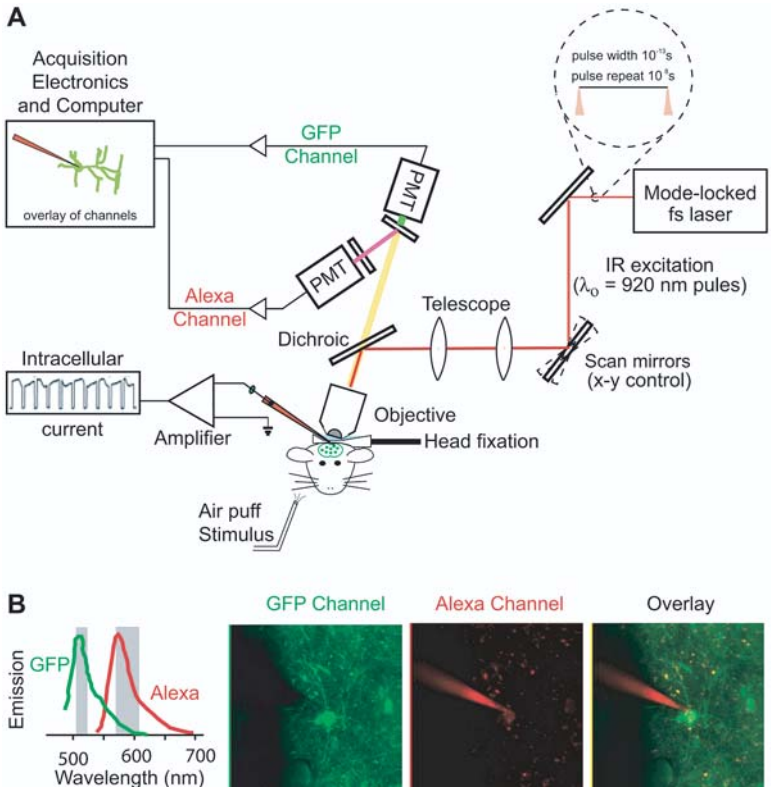

Figure 28.6. In vivo targeted whole-cell recordings of GFP-expressing neurons using TPLSM guidance. (A) The two-photon excitation beam simultaneously stimulated GFP-labeled neurons and the fluorophore Alexa 594 in the patch-clamp pipette. Emission signals from these two sources were spectrally separated by a dichroic mirror and detected separately by two photomultipliers (PMTs). To facilitate the visual guidance of the electrode during its descent towards the targeted cell, the computer generated a composite picture by overlaying the two fluorescence signals using different colors for the cell and the electrode. During final approach of the micropipette electrode on the cell, the resistance of the electrode was used to detect contact between pipette and cell membrane. An example trace shows the change in electrode resistance upon contact of the pipette with the targeted neuron. Since electrode resistance depends on the pressure exerted by the pipette on the cell, modulation of electrode resistance occurred at the heartbeat frequency. (B) TPLSM image of a GFP-expressing interneuron in the superficial layers of vibrissa sensory cortex of mouse. GFP channel: the green channel showing the soma and dendrites of the labeled neuron. Alexa channel: the micropipette that contained the soluble dye Alexa 594. Also shown are the overlay of these two channels and the emission spectra of the two fluorophores. (Adapted from Margrie et al., 2003)

recorded the targeted cell was provided by injecting dye present inside the electrode into the cell; penetrated cells were thus double-labeled (see Fig. 28.6B). At this point, intracellular responses to sensory stimulation were recorded.

The application of TPLSM to guide intracellular electrodes in specific classes of mammalian neurons in vivo will enable future experiments to reach a level of sophistication that was once achieved exclusively in invertebrate preparations and opens the possibility for many future variations of this method. One can anticipate alternative ways to label cells, for instance with retrogradely transported dextran dyes injected into a target zone. Also, this technique could be adapted for intrinsic indicators of intracellular ion concentration (Ohki et al., 2005; Stosiek et al., 2003) to achieve combined intracellular and functional imaging from targeted neurons in vivo.

28.4.1.6 Measurement of Vascular Hemodynamics

Noninvasive blood flow-based imaging techniques are critical to unravel neurovascular coupling (i.e., the relationship between neuronal activity and blood flow). The exchange of nutrients, metabolites, and heat between neurons, astrocytes, and the bloodstream occurs at the level of individual capillaries, vessels 5 to 8 μm in diameter in which red blood cells (RBCs) move in single file. TPLSM, used in combination with electrophysiological recordings, provides the necessary spatial and temporal resolutions to study neurovascular coupling at the level of individual capillaries in vivo. Cortical blood flow can be visualized in anesthetized animals by injecting a fluorescent dye in the bloodstream and by subsequently imaging blood vessels through either a thinned skull or a window-capped craniotomy (Kleinfeld et al., 1998) (Fig. 28.7A). Red blood cells appear as dark spots against the fluorescent plasma (see Fig. 28.7B). Line scans along the length of a capillary of interest can reveal RBC orientation, velocity, and linear density (see Figs. 28.7B and 28.7C). Capillary blood flow in cortex has been visualized in this manner at depths up to 600 μm below the surface of the cerebral cortex. In rat, this allows access to the capillaries of layer 4 neurons, which receive tactile sensory inputs from the large mystacial vibrissae on the face of the rat. This procedure has also been applied in rat olfactory bulb (Chaigneau et al., 2003), a region that contains neurons that respond to odorants. In order to correlate neuronal and hemodynamic activity, electrophysiology is used to make a functional map of neuronal activity in response to a stimulus. The stimulus-induced neuronal activation map can then be compared to blood flow changes made in response to the same stimulus protocol.

Several important conclusions have been drawn from TPLSM studies on neuronal blood flow. First, the natural variability in capillary blood flow was significant and included stalls (see Fig. 28.7D) and even sustained flow reversals. These fluctuations in RBC flow constituted a physiological noise floor that placed limits on the ultimate sensitivity of blood flow-based imaging techniques (Chaigneau et al., 2003). In particular, stimulus-induced changes in cortical RBC speed were found to be on the order of trial-to-trial variability. Nonetheless, significant changes in blood flow around excited neuronal populations were observed to occur both in rat somatosensory cortex and olfactory bulb within 1 to 2 seconds of the application of relevant stimulation (whisker movement and release of odorant, respectively) (see Figs. 28.7E to 28.7H). These

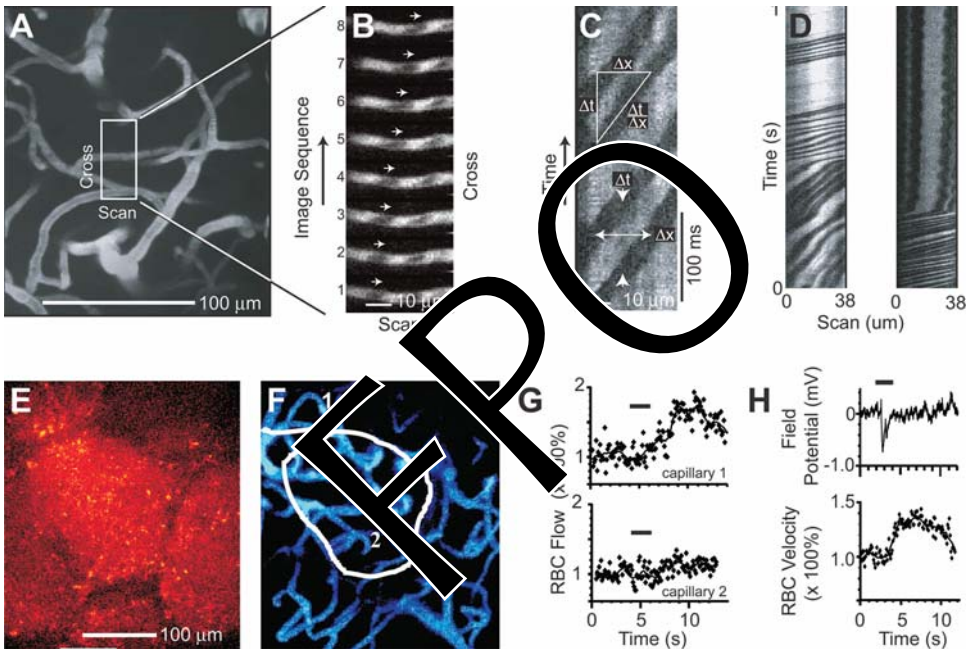

Figure 28.7. TPLSM studies of neurovascular coupling in rat cerebral cortex and olfactory bulb. (A) Horizontal section of capillaries in cortex of a rat constructed from a set of 100 planar TPLSM scans acquired every 1 m at depths of 310 to 410 μm below the pia mater layer. (B) Successive line-scan images of a small vessel acquired every 16 ms. Unstained RBCs showed up as dark shadows against the fluorescently labeled blood plasma. The change in position of an RBC is indicated by the series of arrows. (C) Derivation of instantaneous RBC velocity from a stack of line-scan images made from a 34-μm-long segment of capillary. (D) Examples of irregular flow in 1-second-long line-scan data taken through a straight section of capillary 240 μm below the cortical surface. Notice the change in speed in the first image and the complete stall in the second. (E) Odor-specific populations of a cluster of olfactory bulb neurons called glomerulus were labeled with Oregon Green dextran and imaged with TPLSM. (F) The vasculature of the same region of the olfactory bulb was imaged with TPLSM after injecting the blood stream with fluorescein dextran. The outlines of two adjacent glomeruli were superposed and two capillaries are indicated. (G) One of the two capillaries indicated in G showed an increase in blood flow when an almond odorant was applied to the bulb. The presentation of the stimulus (odorant) is indicated by a black bar. Note that the capillaries are interconnected and separated by ~200 μm. (H) Field potential and blood flow rate measurements in a single glomerulus show that vascular responses occurred 1 to 2 seconds after the neuronal response. (Figure adapted from Kleinfeld et al., 1998, and Chaigneau et al., 2003)

changes in capillary blood flow were well localized to brain regions associated with specific neuronal populations. In the olfactory bulb, differential hemodynamic activity could be distinguished at capillary separation distances of 100 to 200 μm (Chaigneau et al., 2003), though there were no obvious features in the vascular architecture that would support such selective activity. Finally, these studies suggested that the spatial specificity of stimulus-induced rearrangements of blood flow was likely to be based on a decrease in the impedance of a network of capillaries.

28.4.1.7 Long-Term Imaging of Neurodegeneration

The accumulation of amyloid-β plaques in the brain is a hallmark of Alzheimer's disease. Unfortunately, in vivo detection of these plaques remains difficult. Currently, clinical diagnosis relies principally on neurological examinations, with only postmortem confirmation of the underlying pathology (Bacskai et al., 2001). For the development of therapeutic strategies, techniques that allow changes in the neuropathology to be observed over time are critical. Bacskai and associates (Bacskai et al., 2001) recently demonstrated the use of TPLSM to image amyloid-β in the brains of transgenic mice. These mice have been genetically engineered to express a mutant human amyloid-β precursor protein that leads to the formation of plaques similar to those observed in humans with Alzheimer's disease. These plaques were fluorescently labeled by topically applying Thioflavine S or fluorescein-labeled anti-amyloid-β antibodies through a small cranial window over the brain. The vasculature was further labeled by intravenous injection of Texas Red-dextran. Two-photon imaging revealed amyloid-β plaques as well as amyloid accumulation around cerebral vessels (i.e., amyloid angiopathy) (Figs. 28.8A through 28.8C). This technique was then used to test the efficacy of immunotherapy for clearing existing amyloid-β plaques. Animals were imaged before and several days after treatment with an antibody against amyloid-β, administered topically to the brain. The fluorescent vascular images were used as a reference to ensure the same brain areas were imaged before and after treatment. Previous histological studies had observed that immunotherapy reduced plaque accumulation in transgenic mice but could not determine whether old plaques were cleared, new ones prevented, or both. In the work of Bacskai and coworkers (Bacskai et al., 2001), however, the same regions of the brain could be repeatedly imaged, which allowed the effect of the therapy to be observed over time on a plaque-by-plaque basis. Within a few days after treatment, large reductions in the number of plaques were observed while amyloid angiopathy remained unaffected (see Figs. 28.8D and 28.8E). With an appropriate animal preparation that allows repeated imaging over the course of days, weeks, or months, and with easily administered fluorescent markers, TPLSM is a powerful and promising tool for monitoring the progression of neural disease in animal models and will become an important part of testing of future preclinical therapeutic strategies.

28.5 CONCLUSION

Since its introduction in neuroscience about a decade ago, TPLSM has been the object of numerous methodological improvements that have broadened the use of this technique. The next scientific challenges are likely to push the limits of TPLSM towards rapid frame rates in order to image fast neuronal events such as individual action potentials. However, progress in this direction will depend ultimately on the availability of new functional indicators. In TPLSM, the frame rate is determined by the pixel dwell time, which is governed by the minimal acceptable signal-to-noise ratio (Tan et al., 1999). Cells of interest will have to be brightly labeled if they are to be imaged faster and deeper inside the brain. Promising dyes include genetically engineered fluorescent voltage sensors (Siegel & Isacoff, 1997), inducible calcium sensor proteins (Hasan et al., 2004), and second-harmonic activated voltage reporting dyes (Dombeck et al.,

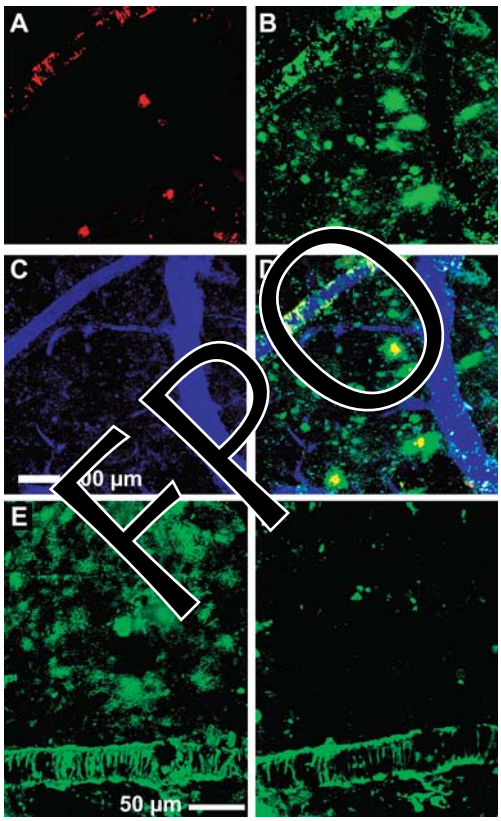

Figure 28.8. Neuropathological assessment of plaque formation and clearance in an animal model of Alzheimer's disease. Projections of two-photon fluorescence image stacks of cerebral amyloid-beta pathology and clearance through immunotherapy in a live, 20-month-old transgenic mouse. (A) Imaging of Thioflavine-S showing amyloid plaques as well as amyloid angiopathy. (B) Visualization of fluorescein-labeled anti-amyloid-beta antibody, showing diffuse amyloid-beta deposits as well as plaques. Both the Thioflavine-S and anti-amyloid-beta antibody were applied to the brain surface for 20 minutes to achieve this labeling. (C) Fluorescence angiography obtained by injecting Texas-Red dextran into the tail vein of the mouse. (D) Merged representation of (A), (B), and (C). (E, F) Images of fluorescently labeled anti-amyloid-antibody reactivity taken before (E) and 3 days after (F) immunotherapy. Amyloid-beta plaques were dramatically reduced, while the amyloid angiopathy was largely unaffected. (Figure adapted from Backsai et al., 2001).

2004). A concomitant issue is how to deliver dyes into neurons of a living animal. Recent techniques that have been evaluated for this task include ballistic delivery of micrometer-size metal particles coated with dye (Kettunen et al., 2002) or electrophoresis (Bonnot et al., 2005). Improvement in the pulse pattern as well as peak intensity of femtosecond lasers will be undoubtedly helpful (Kawano et al., 2003). However, two-photon microscopy is, in practice, limited to $\sim$1,000 μm down in cerebral cortex. To image at this depth, laser power has to be increased so much to counteract scattering that out-of-focus fluorescence resulting from excitation of the surface of the brain above the focal point starts to dominate (Theer et al., 2003).

Despite its tremendous potential, widespread adoption of TPLSM in neurobiology has been limited by its cost, of which a great deal is that of the femtosecond laser, and the fact that only one company markets a complete TPLSM. This situation has forced many investigators to build their own two-photon systems (Tsai et al., 2002). We can hope that in the near future TPLSM will become more readily available and more affordable. This will undoubtedly have beneficial consequences for the development of new contrast agents specifically designed for neurobiological applications with two-photon excitation.

ACKNOWLEDGMENTS

Work in the Kleinfeld laboratory that involves the use of nonlinear microscopy has been supported by grants from the David and Lucille Packard Foundation (99-8326), the NIH (EB003832, MH72570, and NS41096), and the NSF (DBI-0455027). In addition, G.O.C. was supported in part by a NSF/IGERT grant, N.N. was supported in part by a NSF predoctoral training grant, C.B.S. was supported in part by the LJIS training grant from the Burroughs-Wellcome Trust, L.F.S. was supported in part by a NIH/MST grant, and P.S.T. was supported in part by a NIH/NIMH training grant. D.K. takes this opportunity to thank Winfried Denk and Jeff A. Squier to introducing him to nonlinear microscopy and optics.

REFERENCES

Bacskai, B.J., S.T. Kajdasz, R.H. Christie, C. Carter, D. Games, P. Seubert, D. Schenk, and B.T. Hyman. 2001. Imaging of amyloid-beta deposits in brains of living mice permits direct observation of clearance of plaques with immunotherapy. Nature Med. 7: 69–372.

Bacskai, B.J., W.E. Klunk, C.A. Mathis, and B.T. Hyman. 2002. Imaging amyloid-beta deposits in vivo. J. Cereb. Blood Flow & Metab. 22:1035–1041.

Bonnot, A., G.Z. Mentis, J. Skoch, and M.J. O'Donovan. 2005. Electroporation loading of calcium-sensitive dyes into the CNS. J. Neurophysiol. 93:1793–808.

Brecht, M., M.S. Fee, O. Garaschuk, F. Helmchen, T.W. Margrie, K. Svoboda, and P. Osten. 2004. Novel approaches to monitor and manipulate single neurons in vivo. J. Neurosci. 24:9223–9227.

Bullen, A., S.S. Patel, and P. Saggau. 1997. High-speed, random-access fluorescence microscopy: I. High-resolution optical recording with voltage-sensitive dyes and ion indicators. Biophys. J. 73:477–491.

Chaigneau, E., M. Oheim, E. Audinat, and S. Charpak. 2003. Two-photon imaging of capillary blood flow in olfactory bulb glomeruli. Proc. Natl. Acad. Sci. USA. 100:13081–13086.

Denk, W., J.H. Strickler, and W.W. Webb. 1990. Two-photon laser scanning microscopy. Science. 248:73–76.

Denk, W., K.R. Delaney, A. Gelperin, D. Kleinfeld, B.W. Strowbridge, D.W. Tank and R. Yuste. 1994. Anatomical and functional imaging of neurons using 2-photon laser scanning microscopy. J. Neurosci. Methods. 54:151–162.

Denk, W., D.W. Piston, and W.W. Webb. 1995. Two-photon molecular excitation in laser-scanning microscopy. In Handbook of Biological Confocal Microscopy. J.W. Pawley, editor. Plenum Press, New York. 445–458.

Denk, W. and K. Svoboda. 1997. Photon upmanship: Why multiphoton imaging is more than a gimmick. Neuron. 18:351–357.

Dombeck, D.A., M. Blanchard-Desce, and W.W. Webb. 2004. Optical recording of action potentials with second-harmonic generation microscopy. J. Neurosci. 24:999–1003.

Engert, F. and T. Bonhoeffer. 1999. Dendritic spine changes associated with hippocampal long-term synaptic plasticity. Nature. 399:66–70.

Grutzendler. J., N. Kasthuri, and W.-B. Gan. 2002. Long-term dendritic spine stability in the adult cortex. Nature. 420:812–816.

Grynkiewicz, G., M. Poenie, and R.Y. Tsien. 1985. A new generation of Ca2+ indicators with greatly improved fluorescence properties. J. Biol. Chem. 260:3440–3450.

Hasan, M.T., R.W. Friedrich, T. Euler, M.E. Larkum, G. Giese, M. Both, J. Duebel, J. Waters, H. Bujard, O. Griesbeck, R.Y. Tsien, T. Nagai, A. Miyawaki, and W. Denk. 2004. Functional fluorescent Ca2+ indicator proteins in transgenic mice under TET control. PLoS Biol. 2: e163.

Helmchen, F., M.S. Fee, D.W. Tank, and W. Denk. 2001. A miniature head-mounted two-photon microscope: High-resolution brain imaging in freely moving animals. Neuron. 31: 903–912.

Kaiser, K.M.M., J. Lübke, Y. Zilberter, and Sakmann, B. 2004. Postsynaptic calcium influx at single synaptic contacts between pyramidal neurons and bitufted interneurons in layer 2/3 of rat neocortex is enhanced by backpropagating action potentials. J. Neurosci. 24:1319–1329.

Kang, J., G. Arcuino, M. Nedergaard. 2005. Calcium imaging of identified astrocytes in hippocampal slices. In Imaging in Neuroscience and Development, R. Yuste, and A. Konnerth, editors. Cold Spring Harbor Laboratory Press, Cold Spring Harbor. 289–297.

Kawano, H., Y. Nabekawa, A. Suda, Y. Oishi, H. Mizuno, A. Miyawaki, and K. Midorikawa. 2003. Attenuation of photobleaching in two-photon excitation fluorescence from green fluorescent protein with shaped excitation pulses. Biochem. Biophys. Res. Comm. 311:592–596.

Kettunen, P., J. Demas, C. Lohmann, N. Kasthuri, Y. Gong, R.O. Wong, and W.-B. Gan. 2002. Imaging calcium dynamics in the nervous system by means of ballistic delivery of indicators. J. Neurosci. Methods 119:37–43.

Kleinfeld, D., P.P. Mitra, F. Helmchen, and W. Denk. 1998. Fluctuations and stimulus-induced changes in blood flow observed in individual capillaries in layers 2 through 4 of rat neocortex. Proc. Natl. Acad. Sci. USA. 95:15741–15746.

Kleinfeld, D. 2002. Cortical blood flow through individual capillaries in rat vibrissa S1 cortex: Stimulus induced changes in flow are comparable to the underlying fluctuations in flow. In Brain Activation and Cerebral Blood Flow Control, Excerpta Medica, International Congress Series 1235. M. Tomita, editor. Elsevier Science.

Lendvai, B., E.A. Stern, B. Chen, and K. Svoboda. 2000. Experience-dependent plasticity of dendritic spines in the developing rat barrel cortex in vivo. Nature. 404:876–881.

Maletic-Savatic, M., R. Malinow, and K. Svoboda. 1999. Rapid dendritic morphogenesis in CA1 hippocampal dendrites induced by synaptic activity. Science. 283:1923–1927.

Margrie, T.W., A.H. Meyer, A. Caputi, H. Monyer, M.T. Hasan, A.T. Schaefer, W. Denk, and M. Brecht. 2003. Targeted whole-cell recordings in the mammalian brain in vivo. Neuron. 39:911–918.

Martin, S.J., P.D. Grimwood, and R.G. Morris. 2000. Synaptic plasticity and memory: an evaluation of the hypothesis. Annu. Rev. Neurosci. 23:649–711.

Noguchi, J., M. Matsuzaki, G.C.R. Ellis-Davies, and H. Kasai. 2005. Spine-neck geometry determines NMDA receptor-dependent Ca2+ signaling in dendrites. Neuron. 46:609–622.

Ohki, K., S. Chung, Y.H. Ch'ng, P. Kara, and C.R. Reid. 2005. Functional imaging with cellular resolution reveals precise micro-architecture in visual cortex. Nature. 433:597–603.

Purves, D., and R.D. Hadley. 1985. Changes in the dendritic branching of adult mammalian neurones revealed by repeated imaging in situ. Nature. 315:404–406.

Ramón y Cajal, S. 1893. Neue Darstellung vom histologischen Bau des Centralnervensystems. Arch. Anat. Physiol. Anat. Abt. Suppl. 319:428.

Roorda, R.D., T.M. Hohl, R. Toledo-Crow, and G. Miesenbock. 2004. Video-rate nonlinear microscopy of neuronal membrane dynamics with genetically encoded probes. J. Neurophysiol. 92:609–621.

Siegel, M.S., and E.Y. Isacoff. 1997. A genetically encoded probe of membrane voltage. Neuron. 19:735–741.

Stosiek, C., O. Garashuk, K. Holthoff, and A. Konnerth. 2003. In vivo two-photon calcium imaging of neuronal networks. Proc. Natl. Acad. Sci. USA. 100:7319–7324.

Stutzmann, G.E., and I. Parker. 2005. Dynamic multiphoton imaging: A live view from cells to systems. Physiology (Bethesda). 20:15–21.

Svoboda, K., D.W. Tank, and W. Denk. 1996. Direct measurement of coupling between dendritic spines and shafts. Science. 272:716–719.

Tan, Y.P., I. Llano, A. Hopt, F. Wurriehausen, and E. Neher. 1999. Fast scanning and efficient photodetection in a simple two-photon microscope. J. Neurosci. Methods 92: 123–135.

Theer, P., M.T. Hasan, and W. Denk. 2003. Two-photon imaging to a depth of 1000 microm in living brains by use of a Ti:Al2O3 regenerative amplifier. Opt. Lett. 15:1022–1024.

Trachtenberg, J.T., B.E. Chen, G.W. Knott, G. Feng, J.R. Sanes, E. Welker, and K. Svoboda. 2002. Long-term in vivo imaging of experience-dependent synaptic plasticity in adult cortex. Nature. 420:788–794.

Tsai, P. S., N. Nishimura, E. J. Yoder, E. M. Dolnick, G. A. White, and D. Kleinfeld. 2002. Principles, design, and construction of a two photon laser scanning microscope for in vitro and in vivo brain imaging. In In Vivo Optical Imaging of Brain Function. R.D. Frostig, editor. CRC Press, Boca Raton. 113–171.

Woolsey, T.A., and H. van der Loos. 1970. The structural organization of layer IV in the somatosensory region (SI) of mouse cerebral cortex: the description of a cortical field composed of discrete cytoarchitectonic units. Brain Res. 17:205–242.

Yuste, R., and W. Denk. 1995. Dendritic spines as basic functional units of neuronal integration. Nature. 375:682–684.

Zipfel, W.R., R.M. Williams, and W.W. Webb. 2003. Nonlinear magic: multiphoton microscopy in the biosciences. Nat. Biotechnol. 21:1369–1377.

Ziv, N. E., and S.J. Smith. 1996. Evidence for a role of dendritic filopodia in synaptogenesis and spine formation. Neuron. 17:91–102.